ACS APPLIED MATERIALS & INTERFACES
Research Article
www.acsami.org

Thermal Stability of Functional P(S-r-MMA) Random Copolymers for Nanolithographic Applications

Katia Sparnacci,[†] Diego Antonioli,[†] Valentina Gianotti,[†] Michele Laus,*[,†] Giampaolo Zuccheri,[‡] Federico Ferrarese Lupi,[§] Tommaso Jacopo Giammaria,[§] Gabriele Seguini,[§] Monica Ceresoli,[§,⊥] and Michele Perego*[,§]

[†]Dipartimento di Scienze e Innovazione Tecnologica (DISIT), Università del Piemonte Orientale "A. Avogadro", Viale T. Michel 11, 15121 Alessandria, Italy

[‡]Dipartimento di Farmacia e Biotecnologie, INSTM, Centro S3, CNR-Istituto Nanoscienze, Via Irnerio 48, Bologna 40126, Italy

[§]Laboratorio MDM, IMM-CNR, Via C. Olivetti 2, 20864 Agrate Brianza, MB, Italy

[⊥]Dipartimento di Fisica, Università degli Studi di Milano, Via Celoria 16, Milano 20133, Italy

Supporting Information

ABSTRACT: Two strategies are envisioned to improve the thermal stability of the grafted layer and to allow the processing of the random copolymer/block copolymer (RCP/BCP) system at high temperature. From one side, a high-temperature thermal treatment of a commercial α-hydroxyl ω-2,2,6,6-tetramethylpiperidinyloxy functional RCP, namely, TR58, leads to the formation of a stabilized layer able to induce the perpendicular orientation of a symmetric BCP to temperatures higher than 310 °C. On the other side, an α-hydroxyl ω-Br functional RCP, namely, BrR58, with the same molar mass and composition of TR58, was prepared by activator regenerated by electron transfer atom transfer radical polymerization. The resulting brush layer can sustain the self-assembly of the symmetric BCP for processing temperatures as high as 330 °C. In both systems, the disruption of the BCP film, deposited on the grafted RCP layer, occurs because of the formation of bubbles, due to a low-temperature evolution of monomers from the RCP layer. The extent of the low-temperature monomer evolution is higher for TR58 than it is for BrR58 and starts at lower temperatures. For both copolymers, the thermal treatment offsets the low-temperature monomer evolution while still maintaining surface characteristics suitable to induce the perpendicular orientation of the BCPs, thus ultimately extending the range of processing temperatures of the BCP film and consequently speeding the self-organization process.

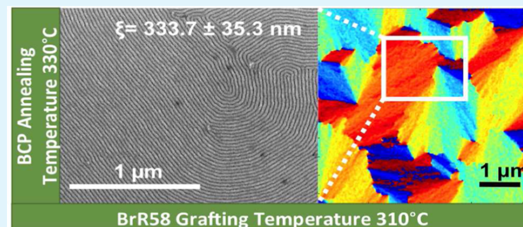

KEYWORDS: *PS-b-PMMA, P(S-r-MMA), self-assembly, rapid thermal processing, thermal stability*

INTRODUCTION

Significant interest is currently focused on nanomanufacturing processes based on block copolymer (BCP) thin films as a viable solution to produce periodic and/or regular nanostructures at relatively low cost.[1−5] Because of their inherent self-assembly propensities, a diversity of morphologies, with periodicities spanning few to hundreds of nanometers, are available. These nanostructured thin films, employed as nanoscale templates for pattern transfer applications, could be exploited in several fields providing a key enabling technology for the fabrication of nanostructured materials[6] and/or functional features in several fields, for instance, photovoltaics, microelectronics, and nanofiltration.

In this regard lamellae and cylinder-forming BCPs, with nanodomains oriented perpendicularly to the underlying substrate, have several advantages in pattern transfer because of the high aspect ratio and sharp side walls of the resulting template.[5] Consequently, the control of the domain orientation represents a key success factor.[7] Preferential wetting of the substrate by one of the blocks, due to the lower interfacial energy, results in parallel orientation of the domains, whereas perpendicular orientation can be achieved with non-preferential interactions at both the bottom and top interfaces. Although modified alkyl chlorosilane[8,9] or ethylene glycol[10] self-assembled monolayers (SAMs) have been used to control the wetting behavior and hence the microdomain orientation of thin films of BCPs, the most common strategy involves the use of functional statistical copolymers, generally referred to as RCP in the literature. Even if statistical would be the proper term to identify this class of copolymers, in the following we will refer to them as RCPs to be consistent with this consolidated habit in the field. In this approach, the concept design underlying the formation of a neutral surface was first described by Mansky[11] and consists in using end-functional poly(A-r-B) RCPs to generate a self-assembled monolayer chemically grafted at the substrate. By finely tuning the composition of the RCP it is possible to prevent preferential wetting and induce the perpendicular orientation of polyA-*b*-

Received: August 8, 2014
Accepted: February 9, 2015
Published: February 9, 2015

ACS Publications © 2015 American Chemical Society

DOI: 10.1021/am509088s
ACS Appl. Mater. Interfaces 2015, 7, 3920−3930

polyB diBCPs. Although this concept has been successively extended,[12−16] leading to a great variety of functional RCPs able to promote not only end-chain but also side-chain grafting reactions,[17,18] the use of functional hydroxyl-terminated poly(styrene-r-methyl methacrylate) (P(S-r-MMA)) RCPs is by far the most common approach to induce perpendicular orientation in polystyrene-*b*-poly(methyl methacrylate) (PS-*b*-PMMA) BCPs. In turn, in spite of the relatively low values of the Flory−Huggins interaction parameter χ, which limits the resolution of domains to ca. 11 nm,[19,20] this class of BCPs represents the current industrial standard for the implementation of novel lithographic approaches based on the integration of self-assembled BCP thin films in conventional photolithographic processes.

In the seminal study proposed by Mansky et al.,[11] the functional P(S-r-MMA) copolymers, with low molar mass and relatively narrow molar mass distribution, were prepared by nitroxide mediated polymerization (NMP) using a hydroxyl (OH) functional unimolecular initiator based on 2,2,6,6-tetramethylpiperidinyloxy (TEMPO) as radical controller. These P(S-r-MMA) copolymers, with tailor-made compositions,[21−23] are terminated on the α-end with a hydroxyl group and on the ω-end with the TEMPO group. The "grafting to" surface functionalization consists in a thermally activated reaction of the hydroxyl group of the functional copolymer with the HO-Si substrates.[24,25] This reaction is generally performed at relatively mild temperatures ($T \ll 200$ °C) in conventional furnaces/ovens and requires long annealing times ranging from several hours to a few days.[11] Recently, it was demonstrated that it is possible to carry out the grafting process in a relatively short time[26] by heating the samples on a hot plate at 250 °C. Then, a very fast grafting procedure, involving the use of a rapid thermal processing (RTP) apparatus, was reported[27] with grafting temperatures up to 310 °C at a heating rate of 20 °C·s^{-1}. Under these conditions, the time necessary to produce the neutral layer is ∼30 s. Interestingly, in the same paper, the authors reported some hints of a thermally induced stabilization of the neutral layer during the high-temperature grafting process, suggesting the possibility to widen the temperature range of the BCP self-assembly. Although the use of solvent-assisted technologies to help the self-assembly of BCPs is widely employed,[28,29] there are several general and specific reasons to process BCPs, and in particular PS-*b*-PMMA, at high temperatures. In general, high-temperature treatments are preferred because they offer the possibility to considerably speed the self-assembly (SA) process and to rapidly access thermodynamically favored morphologies, orientations, and alignments on time scales compatible with industrial processes.[30,29] Moreover at temperatures higher than ∼225 °C, the interfacial interactions at the free surface of PS-*b*-PMMA are balanced,[31] which enables a perpendicular orientation of domains when annealed on a neutral substrate surface. In addition, a film defectivity decrease was observed as the processing temperature increases.[32−34]

The main limitation that often prevents the implementation of high-temperature thermal treatments relies on the thermal stability of the polymeric materials under investigation.[35] Contrary to previous claims,[36] it was recently demonstrated[35] that the thermal stability in bulk and thin film of the P(S-r-MMA) copolymers is definitely lower than that of the PS-*b*-PMMA copolymers. Consequently, the range of accessible temperatures in the processing is mainly limited by the instability of the grafted RCP layer.[35] In principle, the BCPs exhibit a much higher thermal stability that would allow an increase in the processing temperature and achieve the desired level of organization in a time scale well below the requirements of the International Technology Roadmap for Semiconductors.[37]

In this work, we aim to identify suitable strategies to increase the thermal stability of the RCP layer to extend the range of processing temperatures of the BCP film and consequently to speed the self-organization process. For the present investigation, a symmetric BCP was selected because of its higher order−disorder transition temperature than that of an asymmetric BCPs with similar molar mass.[38] This would span a much broader range of processing temperatures and extensively benefit from the increased thermal stability of the RCP layer. Consequently, RCPs with styrene unit fraction of 58% (Figure 1) were employed. This RCP composition was demonstrated as very well-suited[21] in promoting the perpendicular orientation of lamellar-forming symmetric BCPs.

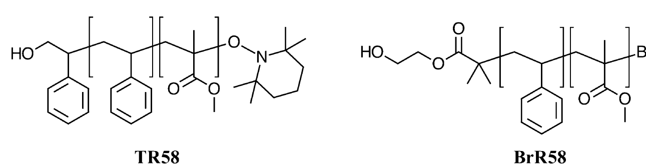

Figure 1. Structures of the α-hydroxyl functional poly(styrene-r-methyl methacrylate) (P(S-r-MMA)) RCPs TR58 and BrR58.

Two strategies are envisioned in this paper to improve the thermal stability of the grafted layer and to allow the processing of the RCP/BCP system at high temperature. A commercial α-hydroxyl ω-TEMPO functional RCP, namely, TR58 is used as a reference system, and an α-hydroxyl ω-bromine functional poly(styrene-r-methyl methacrylate) with the same composition of copolymer TR58 was prepared by Activator ReGenerated by Electron Transfer Atom Transfer Radical Polymerization (ARGET ATRP),[39] namely, BrR58, where the TEMPO moiety is substituted by a bromine atom (Figure 1). The two RCPs TR58 and BrR58 were subjected to several distinct high-temperature thermal treatments to go deep into the thermally induced stabilization mechanism. To probe the effective thermal stability of the grafted RCP layer, symmetric BCP thin films were spin-coated onto the brush layer and subsequently annealed at high temperatures.

EXPERIMENTAL SECTION

Materials. The α-hydroxyl ω-TEMPO functional RCP P(S-r-MMA) with styrene fraction of XS = 0.58 (Mn = 11 400 g·mol^{-1}, polydispersity index (PDI) = 1.64) and the symmetric BCP PS-*b*-PMMA with styrene fraction of XS = 0.50 (Mn = 51 000 g·mol^{-1} and PDI = 1.06, PMMA syndiotactic-rich contents >78%) were purchased from Polymer Source Inc. and used as received. The RCP and the BCP were marked as TR58 and B50, where R and B stand for random and block, respectively, T for TEMPO, and the number represents the percent styrene unit. 2-Hydroxyethyl(2-bromoisobutyrate) (HEBIB), tris(2-(dimethylamino)ethyl)amine (Me_6TREN), copper(II) bromide ($CuBr_2$), tin(II)2-ethylhexanoate ($Sn(EH)_2$), and solvents were purchased from Aldrich and used as received. Styrene and methyl methacrylate were purchased from Aldrich and purified by passing through an inhibitor removal column (Aldrich) before use. The α-hydroxyl ω-Br functional P(S-r-MMA) (BrR58) was synthesized as described in the following paragraph.

Copolymerization of styrene and methyl methacrylate. The α-hydroxyl ω-Br functional RCP BrR58 (Mn = 13 200 g·mol^{-1}, PDI = 1.36, XS = 0.58) was obtained by ARGET ATRP of styrene and

DOI: 10.1021/am509088s
ACS Appl. Mater. Interfaces 2015, 7, 3920−3930

methyl methacrylate initiated by HEBIB and catalyzed by $CuBr_2$/Me_6TREN complex in the presence of $Sn(EH)_2$ as the reducing agent.[39]

In detail, 2.40 mg of $CuBr_2$ (10.3 μmol) and 2.8 μL of Me_6TREN (10.3 μmol) were dissolved in 6.0 mL of degassed anisole and transferred via degassed syringes to a dry Schlenk flask, purged by flushing with nitrogen. Then 8.0 mL of degassed styrene (69.7 mmol), 4.0 mL of degassed methyl methacrylate (37.4 mmol), and 80.0 μL of HEBIB (0.55 mmol) were added, and the mixture was degassed by three freeze−thaw cycles. Next, a purged solution of $Sn(EH)_2$ (84.0 μmol) and Me_6TREN (84.0 μmol) in degassed anisole (1.0 mL) was added, and the mixture was sealed under nitrogen. The polymerization was carried out at 90 °C for 22 h, and then the reaction mixture was cooled to room temperature and diluted with tetrahydrofuran (THF, 5 mL). The copolymer was precipitated into methanol, washed with methanol, and purified by precipitation from THF solution into methanol. The copolymer composition was evaluated by ^{1}H NMR spectroscopy, and the styrene unit fraction resulted in XS = 0.58. The molar mass and first polydispersity index were determined by SEC and resulted in Mn = 13 200 g·mol^{-1} and PDI = 1.36, respectively.

Random Copolymer Characterization. The copolymer composition was evaluated by ^{1}H NMR employing a Jeol Eclipse ECP300 spectrometer. The SEC analysis was performed on THF solutions of the RCPs using a 590 Waters chromatograph equipped with refractive index and ultraviolet detectors and using a column set consisting of Waters HSPgel HR3 and HR4 with a flow rate of 0.6 mL/min. The column set was calibrated against standard PS samples.

Substrate Preparation. Substrates were obtained from (100) oriented Si wafers with a 50 nm thick thermal silicon dioxide layer. Samples with surface of 1 cm^2 were treated with Piranha solution (conc. H_2SO_4/30% H_2O_2 with 3/1 v/v ratio) at 80 °C for 40 min to remove residual organic material and to increase the density of hydroxyl groups at the surface. ***Warning!*** *Piranha solution reacts strongly with organic compounds and should be handled with extreme caution.* The cleaning process of the substrates was completed by rinsing in H_2O, drying in N_2 flow, and then performing an ultrasonic bath in 2-propanol.

Random Copolymer Grafting. Random copolymers BrR58 and TR58 (18.0 mg in solution with 2.00 mL of toluene) were spin-coated on the substrates for 30 s at 4000 rpm. The samples were then RTP thermally treated for 600 s at different temperatures from 170 to 350 °C in N_2 atmosphere to promote the grafting reaction. A further ultrasonic bath in toluene was then performed to remove the nongrafted fraction, and the grafted substrate was dried under N_2 flow. To verify the effective grafting and the presence of unbounded chains, we performed repeated washings in toluene, and we observed no variation of the initial layer thickness. Similarly, we measured the thickness of the grafted RCP layer after annealing the grafted layer at 310 °C for 10 min to simulate the thermal treatment that the layer will experience during the processing of the BCP spun on top of it. No variation of the RCP film was detected after this treatment.

Block Copolymer Deposition. The grafted substrates were spin-coated with a solution of the B50 copolymer (16.0 mg in 2.00 mL of toluene) to obtain polymeric films with a thickness of ∼25 nm. Finally, to promote the organization of BCPs, the resulting samples were subjected to RTP treatment at 310 °C for 60 s.

Rapid Thermal Processing Treatments. The RTP treatments were performed in a Jipelec, JetFirst Series system. The process consists of a three-step treatment (a heating ramp, a plateau, and a cooling ramp) in N_2 atmosphere. The temperature of the sample is constantly monitored in real time by a thermocouple placed underneath the sample. To reach the target temperature in the shortest possible time without over- or under-shooting, the final temperature was set ∼10−20 °C higher than the target one, and as the sample temperature approached the target temperature, the lamp power was progressively reduced. In this way, over- or under-shooting no higher than 1 °C was obtained. In all the thermal treatments, the heating ramp was set at 18 °C·s^{-1}.

Film Characterization. The thicknesses of the random and BCP films were measured by a M-200U spectroscopic ellipsometer (J. A. Wollam Co. Inc.) using a xenon lamp at 70° incident angle. The morphological characterization of the self-assembled BCP films was performed by means of scanning electron microscopy (SEM) in a Zeiss Supra 40 system. To improve the contrast in the SEM images the PMMA phase was selectively removed. The opening of the lamellar patterns was obtained by degrading the PMMA blocks by UV radiation exposure (5 mW·cm^{-2}, λ = 253.7 nm) for 15 min. The samples were treated in oxygen plasma for 60 s at 40 W to remove the PMMA phase and to promote the cross-link of the PS chains. Contact angle measurements were performed using an Attension Theta Optical Tensiometer

Atomic force microscopy characterization of the film surface topography was performed on a Multimode NanoScope V with a J-type piezo scanner (Bruker). Imaging was performed at ambient temperature and humidity in Tapping-mode with NSC15/AIBS MikroMasch noncontact probes. The topography and the phase signals were acquired simultaneously.

Copolymer Characterization. All the thermogravimetric analysis (TGA) and TGA-gas chromatography (GC)-mass spectrometry (MS) analyses were performed using a Mettler TGA/SDTA 851e purged with a steady flow of inert gas at a scanning rate of 20 °C·min^{-1} from room temperature to 1100 °C. For bulk materials, each sample was placed in an open alumina crucible. The polymeric films on the substrate were directly placed on the thermo-balance plate. The TGA of samples TR58 and BrR58 are included as Supporting Information.

The GC-MS analysis was performed using a FINNIGAN TRACE GC-ULTRA and TRACE DSQ. The GC separation was carried out using a Phenomenex DB5−5 ms capillary column (30 m, 0.25 i.d., 0.25 thickness). The injector temperature was set at 250 °C in splitless mode, and helium was used as carrier gas at a constant flow of 1.0 mL·min^{-1}. The MS transfer line and the oven temperatures were set at 280 and 150 °C, respectively.

The evolved gas from TGA was transferred to the GC-MS using the interface described in detail elsewhere.[35] The transfer lines from the TGA to the interface and from the interface to the GC were set at a temperature of 200 °C, the temperature of the interface was 150 °C, and the sampling frequency was 30 s^{-1}. The sampled gas from the loop to the waste was switched after 10 s, and the capacity of the injection loop was 2.5 mL. The MS signal was acquired in electron ionization (EI+) mode with ionization energy of 70.0 eV and at the ion source temperature of 250 °C. The acquisition was performed both in full-scan mode, in the 20−350 $m{\cdot}z^{-1}$ range and in single ion monitoring (SIM) mode by acquiring the signals corresponding to styrene (S) at $m{\cdot}z^{-1}$ = 104 and methyl methacrylate (M) at $m{\cdot}z^{-1}$ = 100.

Direct Exposure Probe Analysis. Direct mass spectrometric analysis of RCPs was performed by the direct exposure probe (DEP) hyphenated with a quadrupolar mass spectrometer (Finnigan TRACE DSQ, Thermo Electron Corporation) that permits a rapid heating of the sample and the collection of the mass signals of the evolved products. Samples were deposited on a filament of rhenium, with a loop at the end, inserted in a ceramic base. A solution was prepared by dissolving the relevant copolymer (2.0 mg) in dichloromethane (10.00 mL). A single drop of 3 μL of this solution was deposited on the filament using a calibrated microsyringe of 10 μL of volume. Then, the solvent was eliminated by heating the filament for 60 s at 50 °C. The filament temperature was regulated by properly adjusting the electric current flowing in the filament.

Two distinct thermal treatments were performed as follows:

(i) simple temperature scan: the sample was subjected to a conditioning step of 90 s at 25 °C followed by a thermal scan from 25 to 800 °C with a heating rate of 1 °C·s^{-1}.

(ii) RCP grafting simulation: the sample was conditioned for 90 s at 25 °C, heated to the required temperature in the range between 225 and 325 °C at 20 °C·s^{-1}, maintained at this temperature for a variable time period, and finally cooled to room temperature by switching off the electric current in the filament. In some experiments, this treatment was followed by a simple temperature scan.

DOI: 10.1021/am509088s
ACS Appl. Mater. Interfaces 2015, 7, 3920−3930

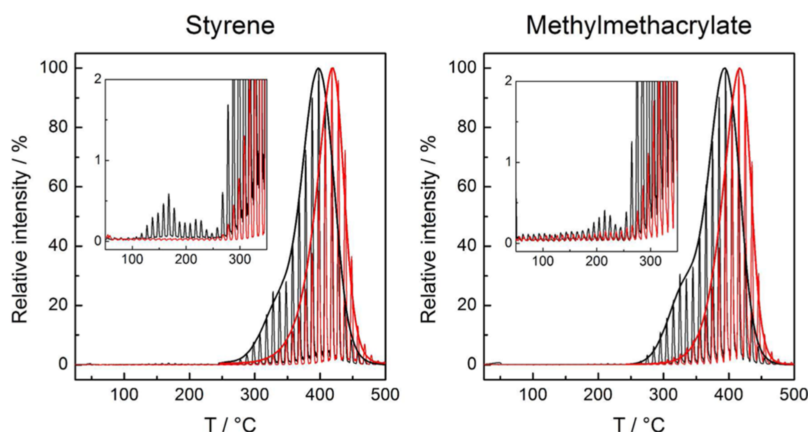

Figure 2. TGA-GC-MS chromatograms for the bulk thermally untreated TR58 (black curves) and BrR58 (red curves) samples with specific reference to the mass peaks at $m \cdot z^{-1}$ 100 and at $m \cdot z^{-1}$ 104, corresponding to methyl methacrylate and styrene, respectively.

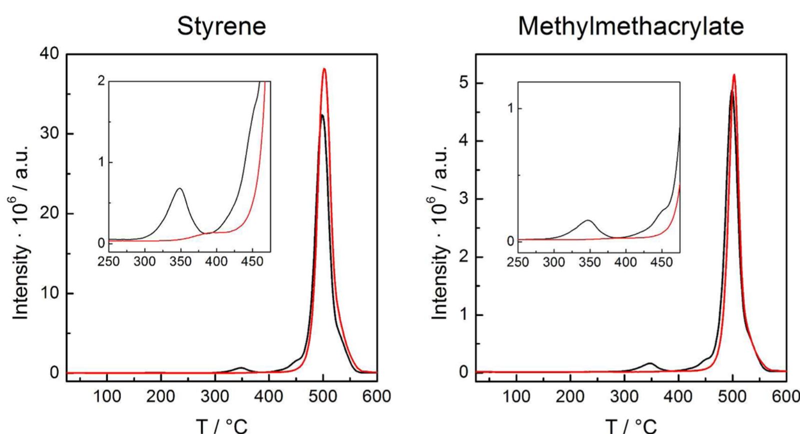

Figure 3. DEP-MS styrene and methyl methacrylate evolution profiles for bulk thermally untreated TR58 (black curves) and BrR58 (red curves). The curves were extracted in selected ion monitoring mode by acquiring the signal corresponding to the typical $m \cdot z^{-1}$ values of styrene at 104 and methyl methacrylate at 100 with the simple thermal treatment (1 °C·s^{-1} heating rate).

MS analyses were performed in EI+ mode, with an ionization energy of 70.0 eV and the ion source temperature of 250 °C. The signal was acquired both in full scan (from 15 to 350 m·z^{-1}) and in SIM by acquiring the signal corresponding to the typical $m \cdot z^{-1}$ values of styrene (S) at 104 and methyl methacrylate (M) at 100. TEMPO signal was registered at 156 $m \cdot z^{-1}$, whereas Br radical was registered at 79 $m \cdot z^{-1}$.

RESULTS AND DISCUSSION

Random Copolymer Stability in Bulk. Figure 2 illustrates the TGA-GC-MS chromatograms of both TR58 and BrR58 in bulk under nitrogen atmosphere with specific reference to the mass peaks at $m \cdot z^{-1}$ 100 and 104, corresponding to methyl methacrylate and styrene, respectively.

The TGA heating rate was 20 °C·min^{-1}, the sampling of the evolved gas occurred every 30 s, and the lines, joining the GC peaks, mark and contour the entire loss profile. As the sensitivity to styrene in the mass detector is definitely higher than that for methyl methacrylate, for a direct comparison, Figure 2 reports the relative peak intensity plots describing the thermal evolution of the two monomers. Apart from TEMPO molecules (not included), styrene and methyl methacrylate monomers correspond to 95% of the released species. The signal intensities corresponding to dimer or trimers, even hybrid in character, are extremely low. This experimental evidence suggests that the degradation of the macromolecules occurs mainly through an unzipping process that leads to the progressive release of the monomers forming the RCP.

The degradation process of sample TR58 starts at ∼140 °C leading to the release of styrene (and TEMPO molecules[35]) and, at ∼10 °C more, methyl methacrylate, whereas the main degradation process starts at ∼240 °C and ends at ∼460 °C with the high-temperature volatilization profile of styrene being similar to the one of methyl methacrylate. In contrast, in the degradation profile of BrR58, no low-temperature losses are observed, whereas, in the main degradation process, the methyl methacrylate and styrene evolutions occur in a closely parallel fashion, at temperatures between 320 and 460 °C. These data clearly indicate that the thermal stability of BrR58 is definitely higher than TR58, in agreement with existing literature concerning the thermal stability of PMMA samples prepared by ATRP[40,41] and NMP.[42] The incidence of abnormal linkages, such as head-to-head and vinylidene ends, is substantially reduced in controlled radical polymerizations compared to conventional free radical polymerizations, thus increasing the thermal stability of the samples prepared by ATRP. The reported TGA curves of bromine-terminated PMMA are very similar to that observed in Figure 2 for BrR58 in which the thermal degradation occurs at ∼375 °C, a temperature identical to that reported in the present paper for the P(S-r-MMA) copolymer prepared by ATRP. However, in the case of NMP,[42] the homolytic cleavage of the C-radical controller bonding

occurs at relatively low temperatures, thus initiating the depolymerization.

The heating rates considered during the TGA analysis are much slower than those commonly used during the RTP processing of these macromolecules. For this reason, the degradation profile was also studied by MS using the DEP tool, which allows[43,44,26] heating of the sample deposited on a filament to be performed at heating rates comprised between 1 and 1000 °C·s^{-1}. Samples TR58 and BrR58 were subjected to the simple temperature scan as described in the Experimental Section. The resulting monomer evolution profiles, from room temperature to 600 °C, are illustrated in Figure 3, and the result is qualitatively similar to the one described in Figure 2 by TGA-GC-MS, although the main losses are shifted to higher temperatures because of the higher heating rate (60 °C·min^{-1}). This indicates that the fast heating rate of the RTP technique moves the onset of the degradation of the RCPs to higher temperature values, thus potentially extending the processing window of the BCP.

Thermal Stability of Thin Random Copolymer Films after the Grafting Treatment. The effect of the grafting treatment was investigated by TGA-GC-MS under dynamic conditions. The samples were prepared by spinning a thin film (~30 nm) of TR58 or BrR58 on the Si substrate. Subsequently, the samples were annealed in RTP by heating the samples at 20 °C·s^{-1} from room temperature to a grafting temperature of between 170 and 350 °C. They were maintained at this temperature for 10 min and then cooled to room temperature at the maximum speed. Finally, a washing step with toluene was performed to remove all the nongrafted material. The relevant film thicknesses are reported in Table 1. In this way, the sample preparation procedure exactly mimics that employed to produce the samples for the successive BCP deposition.

Table 1. TR58 and BrR58 Film Thicknesses after Grafting for 600 s at Different Temperatures

grafting temperature (°C)	TR58 thickness (nm)	BrR58 thickness (nm)
170	2.6	3.5
190	3.4	4.9
210	4.4	6.1
230	4.8	7.3
250	6.2	8.3
270	5.5	8.3
290	5.4	8.4
310	5.4	8.8
330	4.2	8.8
350		8.7

The thermal stability of the grafted polymeric chains was then investigated by TGA-GC-MS analysis. As typical examples, Figure 4 reports the styrene evolution profiles for TR58 and BrR58 after RTP treatment at 230 and 330 °C. The methyl methacrylate evolution parallels that of styrene and is not reported. The same Figure reports the degradation contour profile (dashed line) of TR58 and BrR58 in bulk, for comparison purposes. The overall thermal degradation profile of the two RCPs, monitored through the evolution of the monomers, appears translated toward higher values along the temperature scale in thin films[35] compared to bulk, irrespective of the temperature of the grafting process.

According to literature,[45] this effect is explained considering that, because of the small thickness of the film, the residence

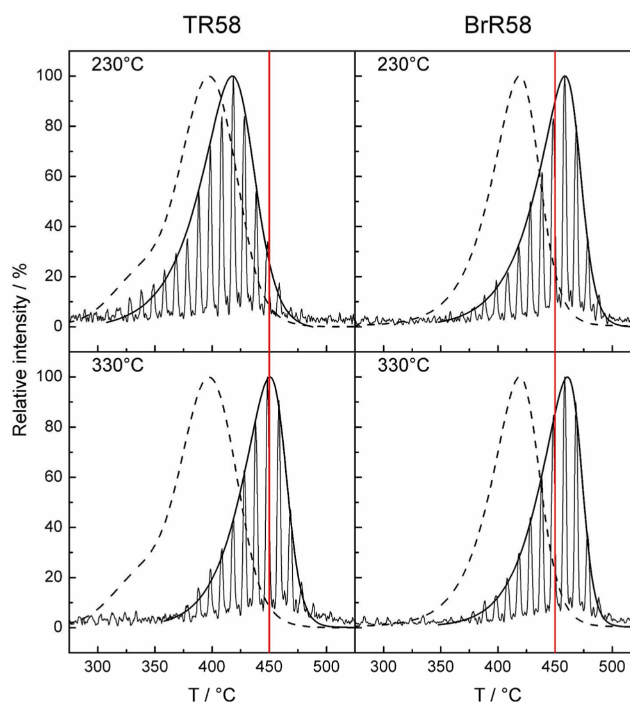

Figure 4. TGA-GC-MS analysis of styrene on TR58 and BrR58 films after the grafting process performed at 230 or 330 °C. The dashed curves represent the corresponding styrene profiles for the bulk samples. The red lines at 450 °C were added as a visual guide.

time in the film of the radicals obtained from chain end scission is too short to allow efficient radical transfer, thus reducing the incidence of the radical transfer processes. As a result, the main degradation moves toward higher temperatures. However, when the layer thickness is between 3 and 8 nm, the degradation curves are identical, within the experimental error.[46] Consequently, a direct comparison between the degradation profiles of the various samples can be reliably made irrespective of the minor thickness differences.

On the other side, the comparison between the samples annealed at 230 and 330 °C reveals quite different behavior of the two polymers. In particular, the degradation profile of the BrR58 sample is not significantly modified when increasing the grafting temperature. Conversely the degradation peak of TR58 samples has remarkably shifted toward high temperature values when increasing the grafting temperature from 230 to 330 °C.

Figure 5 reports collectively the maximum of the degradation peak temperatures for both BrR58 and TR58 samples, taken from the relevant styrene evolution profiles, as a function of the grafting temperature. For the former sample, the maximum of the degradation peak displays a smooth shift toward high temperatures as the grafting temperature increases, confirming our previous observation. In contrast, for the latter sample, a sigmoidal trend is observed with a steep increase, when the grafting process is performed at temperatures higher than 230 °C. This abrupt variation is followed by a smoother increase and an asymptotic stabilization at temperatures higher than 290 °C.

It is important to notice that the thickness of the samples subjected to the above thermal treatment, even at the highest temperatures, undergoes a negligible reduction (~0.3%). In addition, the water contact angle of all these samples is not influenced by the grafting temperature and results in ~82 ±

DOI: 10.1021/am509088s
ACS Appl. Mater. Interfaces 2015, 7, 3920−3930

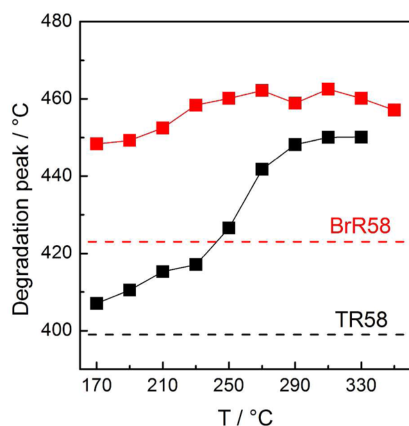

Figure 5. Maximum temperature of the degradation peak for BrR58 and TR58 in the TGA-GC-MS analysis of the styrene evolution as a function of the grafting temperature. The horizontal lines indicate the corresponding degradation temperatures for the bulk samples.

1.0° in all cases, supporting the idea that they can be used to provide a proper neutralized surface for subsequent BCP deposition.

Random Copolymer Grafting Simulation. To better elucidate the effect of the thermal treatment to which the polymers are subjected during the grafting process, a series of analysis was performed by MS using the DEP probe, on samples deposited to the filament and subjected to the RCP grafting simulation treatment as detailed in the Experimental Section. Both TR58 and BrR58 were first heated in the DEP probe to 250 or 325 °C with a heating rate of 20 °C·s^{-1}, maintained at this temperature for different time periods between 10 and 600 s, and then cooled to room temperature. This treatment should simulate the thermal stress to which the RCPs are subjected during the surface grafting process. Next, the samples underwent a simple temperature scan treatment to explore the effect of the thermal annealing at 250 or 325 °C with particular attention paid to the temperature region where the BCP ordering will be performed (250−350 °C). Figure 6 reports the DEP-MS styrene evolution of TR58 and BrR58 subjected to the above thermal treatments. For both copolymer samples, after the treatment at 250 °C for 600 s, the lower-temperature loss peaks are still present. In contrast, when the treatment is performed at 325 °C, the intensities of the styrene loss peaks progressively decrease and are no longer visible after a grafting time of ∼300 s. This result indicates that the thermal degradation process, which causes a monomer loss in the low-temperature region that precedes the main polymer degradation, can be efficiently offset by subjecting both TR58 and BrR58 samples to a high-temperature thermal treatment for relatively short time periods. In addition, combining this result with the trend of the main degradation after the grafting treatments at different temperatures, illustrated in Figures 4 and 5, it may be concluded that during the thermal treatment at high temperatures, homolytic cleavage of the end groups occurs. The resulting radicals, with high local concentration, undergo bimolecular recombination or disproportionation reactions leading to the formation of more stable carbon−carbon bonds, thus in turn improving the overall thermal stability of the RCP chains.

Effective Stability of the Random Copolymer Thin Film after Block Copolymer Deposition. To test the effective stability of the RCP layer, a symmetric BCP thin film was deposited on top of the brush layer obtained by grafting the TR58 and BrR58 RCP thin films at temperatures ranging from 250 to 330 °C for 10 min. The thickness of the BCP films was between 22 and 28 nm. The assembled stack was finally annealed at 310 °C for 1 min to probe its capability to withstand a severe thermal stress. As recently demonstrated, this temperature represents a limiting processing value for the TR58 RCP when not properly stabilized.[34]

In Figure 7, the SEM plan view images of the self-assembled BCP thin film, obtained at two different magnifications, are reported as a function of the TR58 RCP grafting temperature.

When looking at a small scale area, a well-developed lamellar morphology can be observed in all the samples irrespective of the RCP grafting temperature. However, the observation of larger sample areas reveals the occurrence of inhomogeneities in the film. In particular, in the case of the RCP annealed at 250 °C, dark spots are randomly distributed over the entire film indicating the occurrence of some film degradation.[34] Interestingly, in the case of the RCP grafted at 290 °C, no

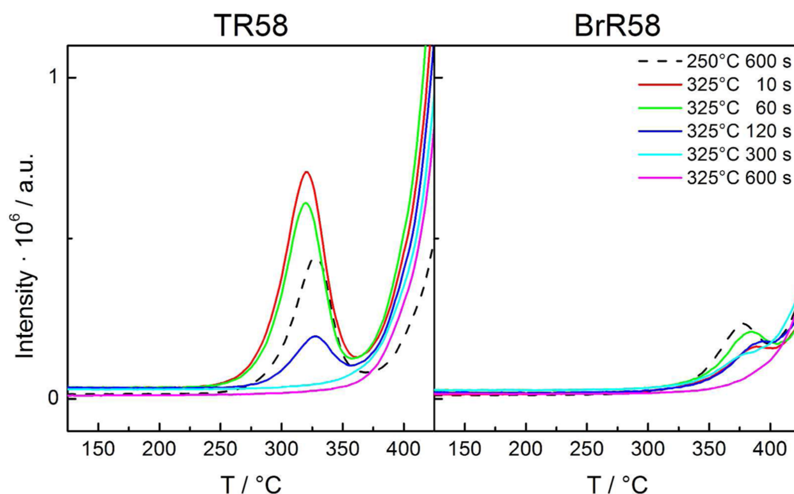

Figure 6. Styrene evolution profile for TR58 and BrR58 subjected to the following thermal treatments. The samples were first heated, with a heating rate of 20 °C·s^{-1}, in the mass spectrometer to 250 °C and maintained at this temperature for 600 s (dashed line) or to 325 °C and maintained at this temperature for different time periods and then cooled to room temperature. Finally the samples were analyzed with a heating rate of 1 °C·s^{-1}.

DOI: 10.1021/am509088s
ACS Appl. Mater. Interfaces 2015, 7, 3920−3930

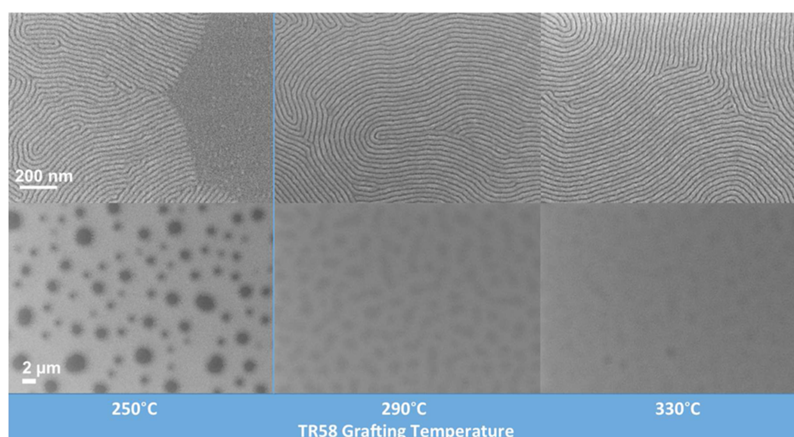

Figure 7. SEM plan view images of the self-assembled BCP thin film as a function of the TR58 RCP grafting temperature obtained at two different magnifications.

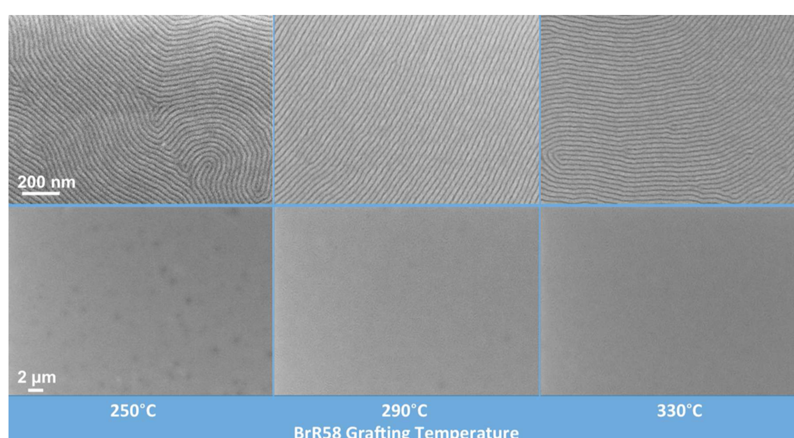

Figure 8. SEM plan view images of the self-assembled BCP thin film as a function of the BrR58 RCP grafting temperature obtained at two different magnifications.

discontinuity in the film is observed. On a large area, local variations in the contrast of the image are evident, representing a warning sign of the degradation process, but no film disruption occurred. The magnified SEM images indicate that the lamellar morphology is preserved even on the dark spots of the film. When the sample is annealed at 330 °C, the homogeneity of the film further increases, and only very limited modification of the contrast is visible in the large-area SEM image. The depicted system evolution perfectly correlates with the progressive stabilization of the TR58 RCP when annealed at high temperature as shown in Figure 5. A similar SEM investigation is reported in Figure 8 for the BrR58 RCP.

The large-area SEM images provide no evidence of degradation phenomena occurring in the film. The enlarged SEM images demonstrate the occurrence of phase separation in the BCP layer and testify to the perpendicular orientation of the lamellar nanodomains with respect to the substrate. The comparison between the data illustrated in Figures 7 and 8 clearly indicates that the thermal stability of BrR58 is definitely higher than that of TR58, in perfect agreement with the degradation results discussed in the previous sections.

The collected data indicate that, when grafting the RCPs at 330 °C, the BCP thin films, deposited on top and thermally treated at 310 °C for 60 s, are stable and homogeneous with a high level of lateral order. It is worth mentioning that this processing temperature of the BCP cannot be achieved when the RCP is grafted at lower temperatures due to the formation of damaged areas randomly distributed on the surface of the sample.[34,35] This fact suggests that by treating the RCP at 330 °C, it could be possible to further increase the annealing temperature of the BCP layer and to speed up the self-assembly process achieving higher correlation length values.

Figure 9 compares the results obtained in the case of BCP thin films deposited on a TR58 RCP brush layer grafted at 330 °C for 10 min. The BCPs were annealed for 1 min at temperatures ranging from 310 to 350 °C. It is important to notice that ordering of the BCP occurs also at this high temperature because of the weak temperature dependence of the Flory−Huggins parameter for PS-*b*-PMMA copolymers.[47] The SEM plan view images highlight a progressive disruption of the polymeric film when increasing the annealing temperature of the BCP. As it can be easily inferred from the SEM plan view images reported in Figure 9, the degradation process of the polymeric stack is similar to the one observed in the case of a TR58 RCP brush layer grafted at 250 °C with the formation of dark spots, which gradually evolve when increasing the annealing temperature and period of time.[34]

A detailed investigation of the degraded areas was performed by AFM analysis. The AFM images, reported in Figure 10, provide information about the morphology of the BCP film after the high-temperature treatments. Upon annealing the BCP film at 310 °C, few local inhomogeneities are evident as

DOI: 10.1021/am509088s
ACS Appl. Mater. Interfaces 2015, 7, 3920−3930

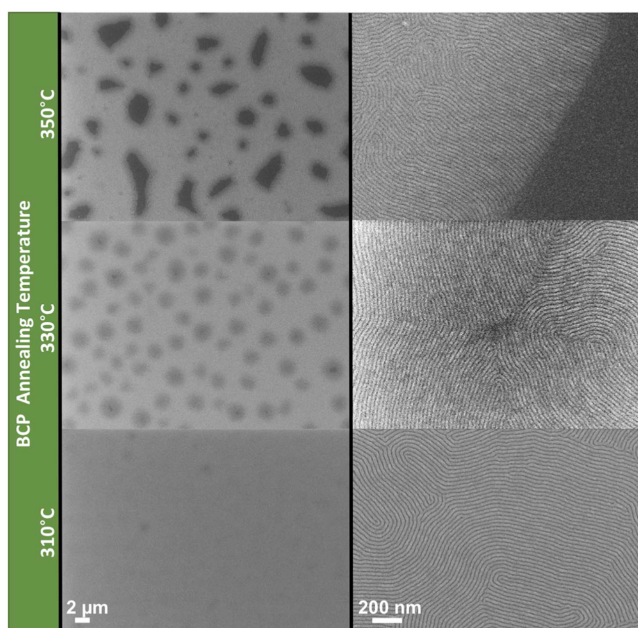

Figure 9. SEM plan view images of TR58 samples treated for 10 min at 330 °C and then processed at different temperatures for 1 min, once B50 was spun. (right) An enlargement of a small area of the corresponding images on the left.

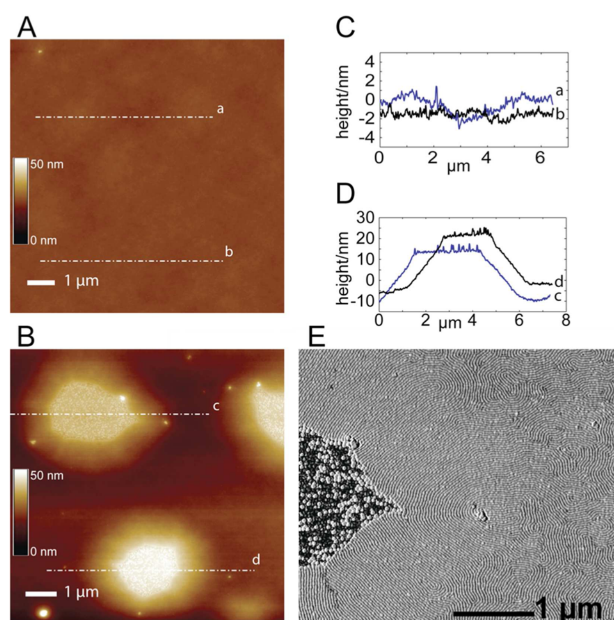

Figure 10. AFM analysis of B50 film annealed at different temperatures for 1 min. The BCP film was prepared on TR58 treated at 330 °C for 10 min. (A) Tapping-mode topographic image showing the film after annealing at 310 °C for 1 min. (B) Tapping-mode topographic image of BCP film annealed at 350 °C for 1 min. (C, D) Traces of the height profiles along the sections marked in panels A and B, respectively. (E) Detail of the AFM tapping-mode phase signal showing the organization of lamellae in the proximity of the ruptured area on the BCP film annealed at 350 °C.

raised point-like areas (Figure 10A). The copolymer layer starts corrugating as highlighted by the height profiles (Figure 10C) along the sections marked in panel A. The film does not break, and the local arrangement of lamellae does not appear significantly different in the flat areas.

Annealing at 330 °C produces a large number of relatively small ruptured areas in the film with aligned lamellae arranged perpendicularly to the edges of the rupture (data not shown). When the film is annealed at 350 °C, ruptured areas appear larger than those in the sample annealed at 330 °C (Figure 10B). These areas are ~25 nm higher than the nanostructured flat copolymer film and present a very flat top portion (Figure 10D). Additionally, several raised pointlike inhomogeneities arise in the flat areas of the copolymer film. Moreover, the regions of the film rising to the degraded areas display an increased level of structural order than the portions of the film at a distance from these regions, often displaying lamellae arranged perpendicularly to the edge of the cracks (Figure 10E).

The correlation length value measured in the BCP film processed at 310 °C is 250.9 ± 30.7 nm. Nevertheless, as revealed by AFM analysis, this increase in the lateral order is accompanied by a corrugation of the polymeric film that could represent a severe limitation in the pattern transfer exploitation.

Figure 11 illustrates the results obtained for the analogous experiment performed on the BrR58 RCP brush layer thermally

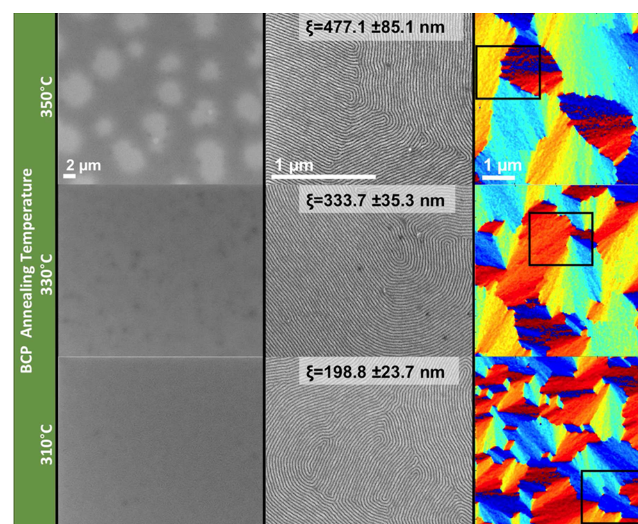

Figure 11. (left) The SEM plan view images of BCP films deposited on the BrR58 brush layer (grafted at 330 °C for 10 min) and subsequently processed at 310, 330, and 350° for 1 min. (right) The color maps obtained from the SEM images corresponding to the same samples are reported. (center) The enlargements of a small area of the SEM images corresponding to the color maps reported in the right column.

treated at 330 °C for 10 min. In the left column in Figure 11, the SEM plan view images of the BCP thin films annealed at 310, 330, and 350 °C are reported. When the annealing temperature of the BCP layer was raised from 310 to 330 °C, no significant variations in the homogeneity of the BCP film are observed. Conversely, the SEM image of the sample annealed at 350 °C shows large areas of well-ordered lamellar pattern, with several bright micrometer-size spots appearing. The color maps obtained from the SEM images corresponding to these samples are reported in the right column of Figure 11. The images provide a direct visualization of the progressive grain coarsening occurring when increasing the annealing process. The central column collects the enlargements of the portion of the SEM images [black rectangle] corresponding to the color

DOI: 10.1021/am509088s
ACS Appl. Mater. Interfaces 2015, 7, 3920–3930

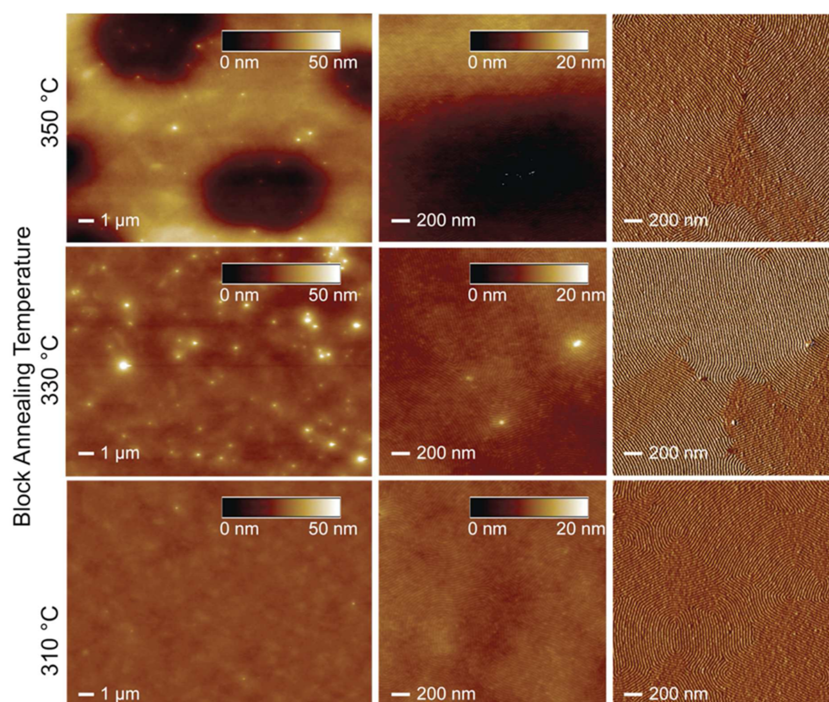

Figure 12. AFM analysis of B50 films annealed at different temperatures for 1 min after being spun on BrR58 treated at 330 °C for 10 min. (inset) The heights of the topographic features and their sizes are coded according to the color tables and scale bars. The tapping-mode phase signal images corresponding to the areas in the central column are outlined in the right column.

maps reported in the right column. The correlation length values are reported in the central column of Figure 11.

Clearly, the increase in the annealing temperature of the BCP films results in a significant improvement of the lateral order, with correlation length values that are 2−3 times higher than those previously reported on the same BCP system.[34] Nevertheless, AFM analysis of the annealed BCP surface, reported in Figure 12, shows that two kinds of surface inhomogeneities arise after increasing the annealing temperature from 310 to 330 and 350 °C. The BCP film annealed at 310 °C shows an unperturbed flat surface with only very moderate long-range corrugations (Figure 12, last row). Occasionally, raised pointlike inhomogeneities are found at isolated locations on the surface. Annealing the films at 330 °C for 1 min results in a significant increase in the number of raised pointlike localized inhomogeneities, while the large-scale appearance of the film is still relatively flat and unperturbed (Figure 12 central row), confirming the enhanced stability of the B50 film when spun on the BrR58 brush layer. Annealing at 350 °C for 1 min generates a number of micrometer-sized film inhomogeneities (Figure 12 first row), as already evidenced by SEM analysis (Figure 11).

AFM images indicate that the nature of these inhomogeneities is significantly different from the film ruptures observed in the case of the B50 BCP film spun on TB58 brush layer. Upon annealing at 350 °C, the B50 film deposited on the BrR58 brush layer exhibits large concavities without any evidence of film rupture. The lamellar nanoscale structure is preserved, and no significant discontinuities in the lamellar organization are observed along the concavities. Even the film annealed at 350 °C presents small raised pointlike film inhomogeneities, albeit in an apparently smaller number than on the film annealed at 330 °C.

The high-resolution AFM images in Figure 13 revealed that the pointlike inhomogeneities are sharply shaped points with

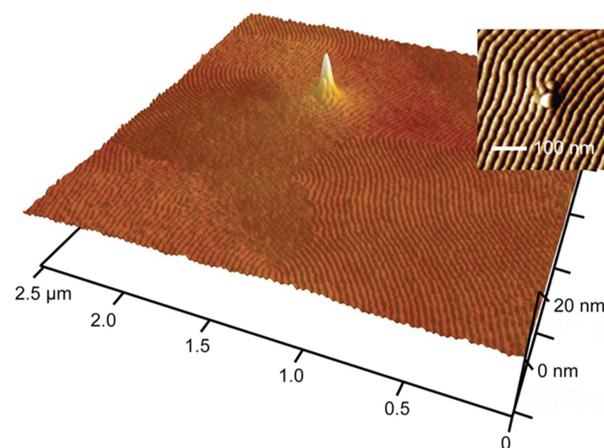

Figure 13. AFM perspective view of a detail of the surface of the B50 film annealed at 330 °C for 1 min on BrR58 and showing a pointlike inhomogeneity.

heights of ∼20−30 nm on the surface of the film and form localized imperfections of the lamellar pattern, corresponding to an abrupt local variation in the number of lamellae. We can hypothesize that, during annealing, the BCP film undergoes some thermal expansion, and the lamellae tend to lengthen. When a lamella interrupts, its local expansion cannot be spread over the entire length of the lamella to accommodate the elongated structure within the network. Consequently, the lamella bumps on top of other lamellae, giving rise to a local "eruption" of the polymeric film that expands above the layer and cannot then relax back in the film upon the subsequent reduction of the temperature. As these inhomogeneities derive

DOI: 10.1021/am509088s
ACS Appl. Mater. Interfaces 2015, 7, 3920−3930

from a variation in the number of lamellae converging on and diverging from the defect point, their formation should be inhibited in topographically registered structures where the number of lamellae is kept constant due to the external constraints imposed by the prepatterned substrate.

■ CONCLUSIONS

To increase the thermal stability of the RCP grafted layer, two converging strategies were described. From one side, a high-temperature thermal treatment of a commercial α-hydroxyl ω-TEMPO functional RCP TR58 leads to the formation of a stabilized layer able to induce the perpendicular orientation of a homogeneous BCP thin film to temperatures as high as 310 °C. On the other side, an α-hydroxyl ω-Br functional RCP BrR58, with the same molar mass and composition of TR58, was prepared and studied. The thermal stability of BrR58 was found inherently higher than TR58. In addition, once subjected to high temperature thermal treatment, the thin copolymer layer deriving from BrR58 was demonstrated to be able to efficiently support the BCP ordering up to 330 °C. Comparison of the thermal analyses and the morphology data clearly reveals that the disruption of the BCP layer, deposited on the grafted RCP layer, occurs because of the formation of bubbles, due to a low-temperature evolution of monomers from the RCP layer. During their growth, these bubbles first start detaching the BCP from the random layer and then break the BCP layer. Both TR58 and BrR58 share the same behavior although the extent of the low-temperature monomer evolution is higher for the former sample and starts at lower temperatures. For both copolymers, the thermal treatment offsets the low-temperature monomer evolution while still maintaining surface characteristics suitable to induce the perpendicular orientation of the BCPs. As the grafting reaction of the RCPs to the silicon wafer can occur in parallel with the stabilizing thermal treatment, this process does not represent an additional step in the processing workflow of the BCPs to obtain nanomanufactured surfaces. This process can be easily integrated into a production line, thus ultimately extending the range of processing temperatures of the BCP film and consequently speeding the self-organization process.

■ ASSOCIATED CONTENT

Supporting Information

TGA and relevant first derivative (DTG) curves of TR58 and BrR58 RCPs in bulk. This material is available free of charge via the Internet at http://pubs.acs.org.

■ AUTHOR INFORMATION

Corresponding Authors

*E-mail: michele.laus@mfn.unipmn.it. (M.L.)

*E-mail: michele.perego@mdm.imm.cnr.it. (M.P.)

Author Contributions

The manuscript was written through contributions of all authors. All authors have given approval to the final version of the manuscript.

Notes

The authors declare no competing financial interest.

■ ACKNOWLEDGMENTS

This research activity was partially funded by the ERANET PLUS "NanoSci-E+" consortium through the NANO-BLOCK project and by the European Metrology Research Programme (EMRP), Project new01-TReND. The EMRP is jointly funded by the EMRP participating countries within EURAMET and the European Union. Partial financial support by PRIN 2010-2011 "Materiali Polimerici Nanostrutturati con Strutture Molecolari e Crystalline Mirate" is acknowledged. Patent protection related to this work is pending.

■ REFERENCES

(1) Li, M.; Ober, C. K. Block Copolymer Patterns and Templates. *Mater. Today* **2006**, *9*, 30−39.

(2) Darling, S. B. Directing the Self-Assembly of Block Copolymers. *Prog. Polym. Sci.* **2007**, *32*, 1152−1204.

(3) Hamley, I. W. Ordering in Thin Films of Block Copolymers: Fundamentals to Potential Applications. *Prog. Polym. Sci.* **2009**, *34*, 1161−1210.

(4) Kim, H. C.; Park, S. M.; Hinsberg, W. D. Block Copolymer Based Nanostructures: Materials, Processes, and Applications to Electronics. *Chem. Rev.* **2010**, *110*, 146−177.

(5) Bates, C. M.; Maher, M. J.; Janes, D. W.; Ellison, C. J.; Willson, C. G. Block Copolymer Lithography. *Macromolecules* **2014**, *47*, 2−12.

(6) Kim, S. O.; Solak, H. H.; Stoykovich, M. P.; Ferrier, N. J.; de Pablo, J. J.; Nealey, P. F. Epitaxial Self-Assembly of Block Copolymers on Lithographically Defined Nanopatterned Substrates. *Nature* **2003**, *424*, 411−414.

(7) Fasolka, M. J.; Banerjee, P.; Mayes, A. M.; Pickett, G.; Balazs, A. C. Morphology of Ultrathin Supported Diblock Copolymer Films: Theory and Experiment. *Macromolecules* **2000**, *33*, 5702−5712.

(8) Peters, R. D.; Yang, X. M.; Kim, T. K.; Sohn, B. H.; Nealey, P. F. Using Self-Assembled Monolayers Exposed to X-Rays to Control the Wetting Behavior of Thin Films of Diblock Copolymers. *Langmuir* **2000**, *16*, 4625−4631.

(9) Peters, R. D.; Yang, X. M.; Kim, T. K.; Nealey, P. F. Wetting Behavior of Block Copolymers on Self-Assembled Films of Alkylchlorosiloxanes: Effect of Grafting Density. *Langmuir* **2000**, *16*, 9620−9626.

(10) Borah, D.; Ozmen, M.; Rasappa, S.; Shaw, M. T.; Holmes, J. D.; Morris, M. Molecularly Functionalized Silicon Substrates for Orientation Control of the Microphase Separation of PS-b-PMMA and PS-b-PDMS Block Copolymer Systems. *Langmuir* **2013**, *29*, 2809−20.

(11) Mansky, P.; Liu, Y.; Huang, E.; Russell, T. P.; Hawker, C. Controlling Polymer-Surface Interactions with Random Copolymer Brushes. *Science* **1997**, *275*, 1458−1460.

(12) Ryu, D. Y.; Shin, K.; Drockenmuller, E.; Hawker, C. J.; Russell, T. P. A Generalized Approach to the Modification of Solid Surfaces. *Science* **2005**, *308*, 236−239.

(13) Shengxiang, J.; Liu, G.; Zheng, F.; Craig, G. S. W.; Himpsel, F. J.; Nealey, P. F. Preparation of Neutral Wetting Brushes for Block Copolymer Films from Homopolymer Blends. *Adv. Mater.* **2008**, *20*, 3054−3060.

(14) Bates, C. M.; Strahan, J. R.; Santos, L. J.; Mueller, B. K.; Bamgbade, B. O.; Lee, J. a; Katzenstein, J. M.; Ellison, C. J.; Willson, C. G. Polymeric Cross-Linked Surface Treatments for Controlling Block Copolymer Orientation in Thin Films. *Langmuir* **2011**, *27*, 2000−2006.

(15) Jung, H.; Leibfarth, F. a.; Woo, S.; Lee, S.; Kang, M.; Moon, B.; Hawker, C. J.; Bang, J. Efficient Surface Neutralization and Enhanced Substrate Adhesion through Ketene Mediated Crosslinking and Functionalization. *Adv. Funct. Mater.* **2013**, *23*, 1597−1602.

(16) Bang, J.; Bae, J.; Löwenhielm, P.; Spiessberger, C.; Given-Beck, S. A.; Russell, T. P.; Hawker, C. J. Facile Routes to Patterned Surface Neutralization Layers for Block Copolymer Lithography. *Adv. Mater.* **2007**, *19*, 4552−4557.

(17) In, I.; La, Y.-H.; Park, S.-M.; Nealey, P. F.; Gopalan, P. Side-Chain-Grafted Random Copolymer Brushes as Neutral Surfaces for Controlling the Orientation of Block Copolymer Microdomains in Thin Films. *Langmuir* **2006**, *22*, 7855−60.

DOI: 10.1021/am509088s
ACS Appl. Mater. Interfaces 2015, 7, 3920−3930

(18) Han, E.; Gopalan, P. Cross-Linked Random Copolymer Mats as Ultrathin Nonpreferential Layers for Block Copolymer Self-Assembly. *Langmuir* **2010**, *26*, 1311−1315.

(19) Seguini, G.; Giammaria, T. J.; Ferrarese Lupi, F.; Sparnacci, K.; Antonioli, D.; Gianotti, V.; Vita, F.; Placentino, I. F.; Hilhorst, J.; Ferrero, C.; Francescangeli, O.; Laus, M.; Perego, M. Thermally Induced Self-Assembly of Cylindrical Nanodomains in Low Molecular Weight PS-b-PMMA Thin Films. *Nanotechnology* **2014**, *25*, 045301.

(20) Ferrarese Lupi, F.; Giammaria, T. J.; Seguini, G.; Vita, F.; Francescangeli, O.; Sparnacci, K.; Antonioli, D.; Gianotti, V.; Laus, M.; Perego, M. Fine Tuning of Lithographic Masks through Thin Films of PS-b-PMMA with Different Molar Mass by Rapid Thermal Processing. *ACS Appl. Mater. Interfaces* **2014**, *6*, 7180−7188.

(21) Ham, S.; Shin, C.; Kim, E.; Ryu, D. Y.; Jeong, U.; Russell, T. P.; Hawker, C. J. Microdomain Orientation of PS- b -PMMA by Controlled Interfacial Interactions. *Macromolecules* **2008**, *41*, 6431−6437.

(22) Han, E.; Stuen, K. O.; La, Y. H.; Nealey, P. F.; Gopalan, P. Effect of Composition of Substrate-Modifying Random Copolymers on the Orientation of Symmetric and Asymmetric Diblock Copolymer Domains. *Macromolecules* **2008**, *41*, 9090−9097.

(23) Han, E.; Stuen, K. O.; Leolukman, M.; Liu, C. C.; Nealey, P. F.; Gopalan, P. Perpendicular Orientation of Domains in Cylinder-Forming Block Copolymer Thick Films by Controlled Interfacial Interactions. *Macromolecules* **2009**, *42*, 4896−4901.

(24) Ballard, C. C.; Broge, E. C.; Iler, R. K.; St John, D. S.; McWhorter, J. R. Esterification of the Surface of Amorphous Silica. *J. Phys. Chem.* **1961**, *65*, 20−25.

(25) Dion, M.; Rapp, M.; Rorrer, N.; Shin, D. H.; Martin, S. M.; Ducker, W. A. The Formation of Hydrophobic Films on Silica with Alcohols. *Colloids Surf., A* **2010**, *362*, 65−70.

(26) Liu, C.-C.; Thode, C. J.; Rincon Delgadillo, P. A.; Craig, G. S. W.; Nealey, P. F.; Gronheid, R. Towards an All-Track 300 mm Process for Directed Self-assembly. *J. Vac. Sci. Technol., B: Microelectron. Process. Phenom.* **2011**, *29*, 06F203.

(27) Ferrarese Lupi, F.; Giammaria, T. J.; Seguini, G.; Ceresoli, M.; Perego, M.; Antonioli, D.; Gianotti, V.; Sparnacci, K.; Laus, M. Flash Grafting of Functional Random Copolymers for Surface Neutralization. *J. Mater. Chem. C* **2014**, *2*, 4909.

(28) Metwalli, E.; Perlich, J.; Wang, W.; Diethert, A.; Roth, S. V.; Papadakis, C. M.; Müller-Buschbaum, P. Morphology of Semicrystalline Diblock Copolymer Thin Films upon Directional Solvent Vapor Flow. *Macromol. Chem. Phys.* **2010**, *211*, 2102−2108.

(29) Sinturel, C.; Vayer, M.; Morris, M.; Hillmyer, M. Solvent Vapor Annealing of Block Polymer Thin Films. *Macromolecules* **2013**, *46*, 5399−5415.

(30) Ferrarese Lupi, F.; Giammaria, T. J.; Ceresoli, M.; Seguini, G.; Sparnacci, K.; Antonioli, D.; Gianotti, V.; Laus, M.; Perego, M. Rapid Thermal Processing of Self-Assembling Block Copolymer Thin Films. *Nanotechnology* **2013**, *24*, 315601.

(31) Mansky, P.; Russell, T. P.; Hawker, C. J.; Mays, J.; Cook, D. C.; Satija, S. K. Interfacial Segregation in Disordered Block Copolymers: Effect of Tunable Surface Potentials. *Phys. Rev. Lett.* **1997**, *79*, 237−240.

(32) Welander, A. M.; Kang, H.; Stuen, K. O.; Solak, H. H.; Müller, M.; de Pablo, J. J.; Nealey, P. F. Rapid Directed Assembly of Block Copolymer Films at Elevated Temperatures. *Macromolecules* **2008**, *41*, 2759−2761.

(33) Perego, M.; Ferrarese Lupi, F.; Ceresoli, M.; Giammaria, T. J.; Seguini, G.; Enrico, E.; Boarino, L.; Antonioli, D.; Gianotti, V.; Sparnacci, K.; Laus, M. Ordering Dynamics in Symmetric PS-b-PMMA Diblock Copolymer Thin Films During Rapid Thermal Processing. *J. Mater. Chem. C* **2014**, *2*, 6655−6664.

(34) Ceresoli, M.; Ferrarese Lupi, F.; Seguini, G.; Sparnacci, K.; Gianotti, V.; Antonioli, D.; Laus, M.; Boarino, L.; Perego, M. Evolution of Lateral Ordering in Symmetric Block Copolymer Thin Films upon Rapid Thermal Processing. *Nanotechnology* **2014**, *25*, 275601.

(35) Gianotti, V.; Antonioli, D.; Sparnacci, K.; Laus, M.; Giammaria, T. J.; Ferrarese Lupi, F.; Seguini, G.; Perego, M. On the Thermal Stability of PS-b-PMMA Block and PS-r-PMMA Random Copolymers for Nanopatterning Applications. *Macromolecules* **2013**, *46*, 8224−8234.

(36) Borah, D.; Rasappa, S.; Senthamaraikannan, R.; Shaw, M. T.; Holmes, J. D.; Morris, M. The Sensitivity of Random Polymer Brush-Lamellar Polystyrene-b-Polymethylmethacrylate Block Copolymer Systems to Process Conditions. *J. Colloid Interface Sci.* **2013**, *393*, 192−202.

(37) *Emerging Research Materials;* International Technology Roadmap for Semiconductors (ITRS), 2007.

(38) Koo, K.; Ahn, H.; Kim, S.-W.; Ryu, D. Y.; Russell, T. P. Directed Self-Assembly of Block Copolymers in the Extreme: Guiding Microdomains from the Small to the Large. *Soft Matter* **2013**, *9*, 9059−9071.

(39) Jakubowski, W.; Min, K.; Matyjaszewski, K. Activators Regenerated by Electron Transfer for Atom Transfer Radical Polymerization of Styrene. *Macromolecules* **2006**, *39*, 39−45.

(40) Granel, C.; Dubois, P.; Jérome, R.; Teyssié, P. Controlled Radical Polymerization of Methacrylic Monomers in the Presence of a Bis (ortho-chelated) Arylnickel (II) Complex and Different Activated Alkyl Halides. *Macromolecules* **1996**, *29*, 8576−8582.

(41) Moineau, G.; Minet, M.; Dubois, P.; Teyssie, P.; Senninger, T.; Jerome, R. Controlled Radical Polymerization of (Meth)acrylates by ATRP with $NiBr_2(PPh_3)_2$ as Catalyst. *Macromolecules* **1999**, *32*, 27−35.

(42) Colombani, D.; Steenbock, M.; Klapper, M.; Mullen, K. 1,3,5,5-Tetraphenyl-D3−1,2,4-triazolin-2-yl Radical-Properties in the Controlled Radical Polymerization of Poly(methyl methacrylate) and Polystyrene. *Macromol. Rapid Commun.* **1997**, *18*, 243−251.

(43) Lehrle, R.; Shortland, A. Reproducibility of Filament Pyrolysers: Influence of Sample Deposition and Other Factors. *Eur. Polym. J.* **1993**, *29*, 1277−1282.

(44) Lehrle, R.; Atkinson, D. J.; Bate, D.; Gardner, P.; Grimbley, M.; Groves, S.; Place, E.; Williams, R. Diagnosis Mechanisms of Oligomers Formation in the Thermal Degradation of Polymers. *Polym. Degrad. Stab.* **1996**, *52*, 183−196.

(45) Manring, L. E. Thermal Degradation of Poly(methyl methacrylate)2. Vinyl-Terminated Polymer. *Macromolecules* **1989**, *22*, 2673−2677.

(46) Gianotti, V.; Antonioli, D.; Sparnacci, K.; Laus, M.; Giammaria, T. J.; Ceresoli, M.; Ferrarese Lupi, F.; Seguini, G.; Perego, M. Characterization of Ultra-Thin Polymeric Films by Gas Chromatography-Mass Spectrometry Hyphenated to Thermogravimetry. *J. Chromatogr., A* **2014**, *1368*, 204−210.

(47) Russell, T. P.; Hjelm, R. P.; Seeger, P. A. Temperature Dependence of the Interaction Parameter of Polystyrene and Poly (methy1 methacrylate). *Macromolecules* **1990**, *23*, 890−893.

DOI: 10.1021/am509088s
ACS Appl. Mater. Interfaces 2015, 7, 3920−3930